J. Mech. Phys. Solids, 1976, Vol. 24, pp. 147 to 169. Pergamon Press. Printed in Great Britain.

ON THE MECHANISMS OF DUCTILE FAILURE IN HIGH-STRENGTH STEELS SUBJECTED TO MULTI-AXIAL STRESS-STATES

By J. W. HANCOCK and A. C. MACKENZIE

Department of Mechanical Engineering, University of Glasgow, Glasgow G12 8QQ, Scotland

(*Received 24th September* 1975)

SUMMARY

THE STRAIN required to initiate ductile failure in three low-alloy, quenched and tempered steels has been determined in multi-axial stress-states. The ductility was found to depend markedly both on the orientation of the stress system with respect to the rolling direction and on the tri-axiality of the stress-state. In some cases, ductile failure occurred at plastic strains which were only a few times the yield strain.

Metallographic studies have been used to compare the size, shape and orientation of the holes which cause failure initiation with the isotropic continuum analysis of F. A. MCCLINTOCK (1968). The application of ductile-fracture models to directional steels is discussed with particular reference to the effects of directionality and stress-state on the condition for flow localization to occur between holes.

NOTATION

$\bar{\sigma}$	effective stress
$\sigma_1, \sigma_2, \sigma_3$	principal stresses
de_1^p, de_2^p, de_3^p	principal plastic strain increments
$d\bar{e}^p$	increment of effective plastic strain
σ_m	mean stress
R	profile radius of notched tensile-specimen
r	radial co-ordinate
d	radius of the minimum cross-section of a notched tensile-specimen
d_0	initial value of d
S.T.	short transverse direction with respect to the rolling direction
L.T.	long transverse direction with respect to the rolling direction
$\bar{e}^p$	effective plastic strain
σ_r	radial stress
σ_θ	hoop stress
σ_z	axial stress
$\bar{e}^f$	effective plastic strain to initiate failure
l_a	current dimension of a unit cell surrounding a void in the direction of the hole major axis
l_b	current dimension of a unit cell surrounding a void in the direction of the hole minor axis

l_a^0	initial value of l_a
l_b^0	initial value of l_b
a	semi major axis of elliptical hole
b	semi minor axis of elliptical hole
F_a	hole-growth factor in the direction of the hole major axis
F_b	hole-growth factor in the direction of the hole minor axis
F_a^f	value of F_a at hole coalescence in the a-direction
F_b^f	value of F_b at hole coalescence in the b-direction
n	hardening exponent in the Ludwig stress–strain relation
σ_0	normalizing stress in the Ludwig stress–strain relation
α	constant
$\bar{e}_n$	effective plastic strain to nucleate a void
de_{dil}	increment of dilatational strain
e_r	radial strain
e_θ	hoop strain
f_0	initial volume fraction of voids
P_h	load for homogeneous deformation
σ_y	yield stress in uni-axial tension
P_l	load for localized flow
h	inclusion colony spacing in the short transverse direction
w	inclusion colony spacing in the rolling direction
t	thickness of a shear band
τ	shear stress
m	eccentricity of elliptical hole
R	mean radius of elliptical hole
κ	constant
$O(x, y)$	orthogonal rectangular cartesian axes
α'	angle between σ_1-direction and the x-axis
ϕ	angle between semi major axis of the ellipse and the x-axis
t'	time
μ	viscosity

1. INTRODUCTION

THE ABILITY of metals to flow plastically is an important property in their use as structural materials. Despite the fact that many structures are designed on an *elastic* basis, the presence of stress concentrators inevitably causes yielding. Yield and subsequent plastic flow may limit the high stresses that would otherwise be produced, but they replace what would have been a *stress* concentration by a *strain* concentration. In such situations, it is essential to ensure that the material has sufficient ductility to prevent failure in a ductile mode. However, the stress systems involved are rarely simple, and, in order to design and use materials effectively in these conditions, it is necessary to be able to test and understand their behaviour in complex stress-states.

This investigation has largely been concerned with the effect of stress-state on the effective plastic strain required to initiate ductile failure in a range of materials including three low-alloy, quenched and tempered steels. Metallographic studies of the events leading to failure initiation have been concentrated on one of these steels,

designated Q1, although comparison with the ductile-failure mechanisms of other materials has also been made in order to facilitate a discussion of the observed stress-state dependence.

The strain to initiate failure as a function of stress-state is of course directly useful in a comparison of the properties of possible materials for a given application. However, MACKENZIE, HANCOCK and BROWN (1976) have also applied the data to the prediction of ductile-failure initiation in the plastic-strain field ahead of cracks and notches. In such situations, it is generally accepted (MCCLINTOCK, 1956, and RITCHIE, KNOTT and RICE, 1973) that it is not sufficient for a failure stress and/or strain to be reached at a single point, but that the failure criterion must involve a certain *minimum amount of material which is characteristic of the scale of physical events leading to local failure.* Estimates of the nature and the scale of these events form a significant part of the work reported here.

2. PLASTIC FLOW AND THE STRESS-STATE

In metals, plastic flow is induced by shear stresses, which cause dislocation movement, and which may be measured by an effective stress $\bar{\sigma}$ which is proportional to the root mean-square of the principal shear stresses, viz.

$$\bar{\sigma} = [\tfrac{1}{2}\{(\sigma_1-\sigma_2)^2+(\sigma_2-\sigma_3)^2+(\sigma_3-\sigma_1)^2\}]^{\frac{1}{2}}. \tag{1}$$

The extent of plastic flow is usually expressed by an analogous quantity, the effective plastic strain increment $d\bar{e}^p$ which is proportional to the root mean-square of the principal plastic shear strain increments, viz.

$$d\bar{e}^p = [\tfrac{2}{9}\{(d\bar{e}_1^p-d\bar{e}_2^p)^2+(d\bar{e}_2^p-d\bar{e}_3^p)^2+(d\bar{e}_3^p-d\bar{e}_1^p)^2\}]^{\frac{1}{2}}, \tag{2}$$

the effective stress and plastic strain being connected by a stress–strain relation (such as the Ludwik relation (11)). Both $\bar{e}^p$ and $\bar{\sigma}$ are unaffected by a third important parameter, the mean stress

$$\sigma_m = \tfrac{1}{3}(\sigma_1+\sigma_2+\sigma_3), \tag{3}$$

which may, however, be combined with $\bar{\sigma}$ into a single non-dimensional parameter $\sigma_m/\bar{\sigma}$ which characterizes a stress-state and is a measure of its 'tri-axiality'. These are the parameters which largely feature in the subsequent discussion here of ductile failure.

3. EXPERIMENTAL PROGRAMME

3.1 *Mechanical testing*

In order to vary $\sigma_m/\bar{\sigma}$ experimentally, tests were carried out on circumferentially-notched tensile specimens. To obtain the values of $\bar{e}^p$ and $\sigma_m/\bar{\sigma}$ where failure occurs, the results of BRIDGMAN's (1952) analysis have been used. This analysis was originally performed for a necked tensile-specimen but it may be applied as an approximation to the pre-notched specimens after fully-plastic conditions have been reached. (A discussion of the applicability of BRIDGMAN's (1952) analysis to pre-notched specimens has been given by EARL and BROWN (1976).) The main features of the analysis are that $\bar{e}^p$ is constant across the mean cross-section, but the radial, hoop and axial

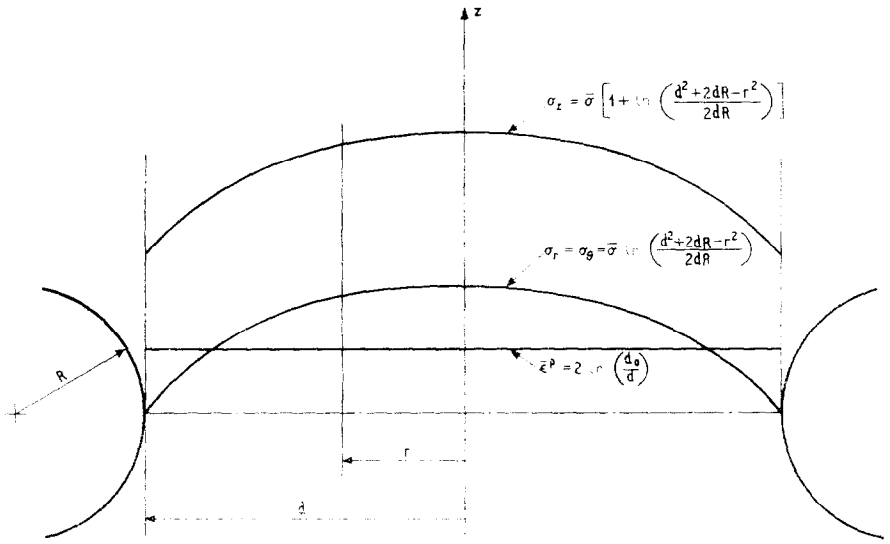

FIG. 1. The stress distribution in a pre-notched tensile specimen (after BRIDGMAN (1952)).

stresses (σ_r, σ_θ, and σ_z, respectively) vary across the section as shown in Fig. 1. The value of $\sigma_m/\bar{\sigma}$ rises from $\frac{1}{3}$ at the surface to a maximum value on the axis of the specimen, that is

$$(\sigma_m/\bar{\sigma})_{max} = \tfrac{1}{3} + \ln (d/2R + 1), \tag{4}$$

where R is the profile radius of the circumferential notch and d is the radius of the minimum cross-section (see Fig. 2). Thus, the stress-state is defined by the geometry of the specimen, and the effective plastic strain is

$$\bar{e}^p = 2 \ln (d_0/d), \tag{5}$$

where d_0 is the initial value of d. The dimensions of the specimen used in the present work are given in Fig. 2, the different notch-geometries being labelled A to E.

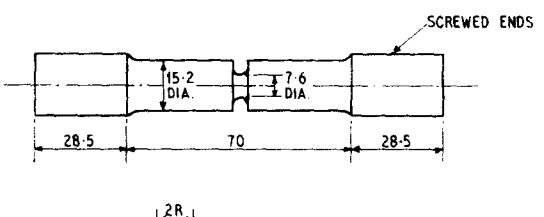

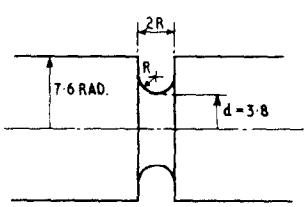

SPECIMEN	R
A	3·80
B	2·54
C	1·90
D	1·27
E	6·34

FIG. 2. The geometry and dimensions of the notched tensile-specimens. (All specimen dimensions in mm.)

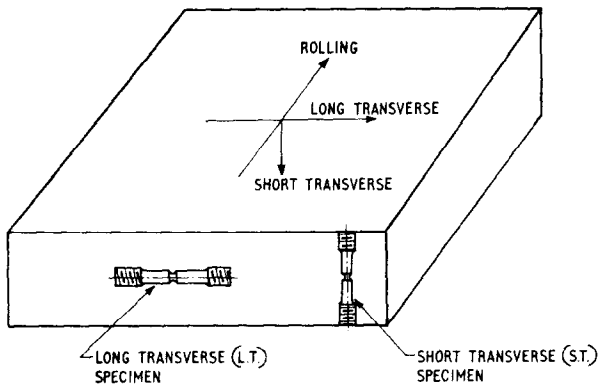

FIG. 3. The orientation of the notch tensile-specimens taken from the rolled plate.

Specimens were machined from both the long transverse and short transverse directions in rolled steel plate as shown in Fig. 3. The tests were carried out in an Instron 250 kN servo-hydraulic testing machine using a strain-gauge extensometer to monitor continuous changes in the minimum diameter of the notch, and a second transducer mounted across the notch to control the axial displacement rate.

Figure 4 shows the results of a series of notched tensile-tests with different notch-geometries in which the average axial stress (the load divided by the instantaneous cross-sectional area, measured externally) is plotted against $\bar{e}^p$ calculated from (5). After the initial elastic response, the average stress rises as the material strain-hardens and then drops sharply. The high mean-stresses usually associated with the notches are reflected in the high average axial-stresses for a given strain compared with those

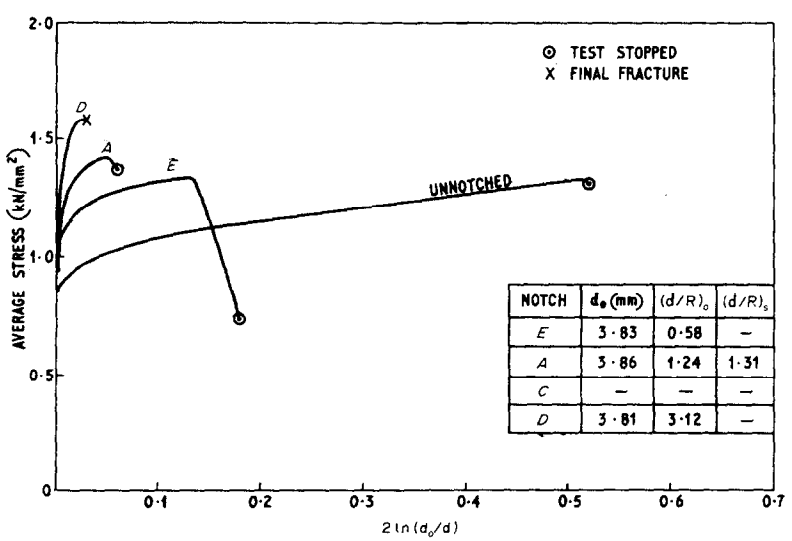

FIG. 4. The average axial stress plotted against 2 ln (d_0/d) for the notch tests of HY130 (S.T.).

for the unnotched specimen. The strain $\bar{e}^f$ at which the average stress drops is here defined as the strain at failure initiation; the physical significance of this event is discussed later. However, it should be noted that $\bar{e}^f$ and the total ductility of the specimens decrease markedly as the tri-axiality increases.

3.2 *Materials*

Three rolled, low alloy, quenched and tempered steels containing approximately 4% Ni and 1% Cr have been used in the present work. The specifications of two of the materials, designated Q1 and HY130, are given in Tables 1 and 2. The third steel, designated ESR, is an electroslag re-melted version of HY130 which was heat-treated to the HY130 specification. Both the HY130 and the ESR steels were treated with Hypercal as an inclusion-shape modifier.

TABLE 1. *Composition of Q1*

Specification of Q1 (% wt. * maximum value)				
C	Mn	Si	S	P
0·18*	0·1–0·4	0·15–0·35	0·015*	0·015*
Ni	Cr	Mo	V	Ti
2·25–3·25	1·0–1·8	0·2–0·5	0·02*	0·02
Co	Cu			
0·03*	0·20			

TABLE 2. *Composition of* HY130

Specification of HY130 (% wt. * maximum value)				
C	Si	Mn	P	S
0·12*	0·20–0·35	0·5–0·9	0·01*	0·015*
Ni	Cr	Mo	V	Ti
4·75–5·25	0·4–0·7	0·30–0·65	0·05–0·10	0·02*
Cu				
0·25				

Electron-probe micro-analysis of Q1 showed inclusions based on Si, Al, and MnS. However, in the HY130 and ESR steels, most inclusions appeared to be rare-earth sulphides (probably Ce as shown by Edax analysis).

In both Q1 and HY130 steels, the inclusions were often found in plate-like colonies in the rolling plane with dimensions in the rolling and long transverse directions approximately equal. Most of the colonies, (such as the one shown in Fig. 5), have major diameters between 8–20 μm but some were as large as 100 μm. In addition, there was extensive segregation of the alloying elements into bands, parallel to the rolling direction. Unlike the conventionally prepared Q1 and HY130 alloys, the comparable

alloy made by electroslag re-melting did not show marked segregation, nor were there stringers of inclusions present, although the total volume fraction of inclusions appeared to be comparable with the other two steels.

3.3 *Metallography*

To study metallographic features associated with failure initiation, tests were stopped after different plastic strains, and specimens, sectioned longitudinally near the centre plane, were examined unetched. A further 50–100 μm thickness was then removed by carefully repeating the final stages of polishing, and the specimen re-examined. This procedure was repeated until at least four sections had been examined in each specimen.

In specimens examined after the drop in average stress, there was a large central crack as shown in Fig. 6 and a loss in load-bearing cross-section: in specimens examined before a drop in average stress, there were discrete holes. Q1 specimens examined close to the drop in average stress showed that holes had joined up over a length scale of approximately 200 μm. The linking-up of the larger holes and the subsequent sudden loss in load-bearing cross-section is considered to be a distinct event in the failure process which we have termed *failure initiation.*

The mechanisms of failure initiation for specimens tested with the major principal stress in either the *short* or *long* transverse direction are different, as shown in Figs. 7 and 8. In the case of Q1, tested in the short transverse direction, the event was identified as micro-cracking between large elliptical holes; whereas in the long transverse direction, the tendency was for groups of larger holes to grow to almost complete coalescense. In HY130, in the short transverse direction, failure initiation was associated with micro-cracking between inclusion colonies as shown in Fig. 9. The overall fracture surface which resulted from final failure of HY130 in the short transverse direction is shown in Fig. 10(a); Fig. 10(b) shows the hole growth within an inclusion colony; and Fig. 10(c) shows the linking micro-cracked region which consists of finer-scale hole growth. In the long transverse direction, there was very much more extensive growth of the large holes; and the ESR steel showed similar hole-growth in both the short and long transverse directions.

Sectioning specimens of all the steels at strains well before failure initiation showed that the holes nucleated at inclusions by one of three mechanisms: (i) fracture of the particle-matrix interface, (ii) failure of the particle, or (iii) micro-cracking of the matrix surrounding the inclusion. In all cases, some holes started to form from the larger inclusions at very small strains and continued to form during the subsequent deformation.

In Q1, tested in the short transverse direction, holes were found in A-notch specimens at a strain of 0·05. At this strain, holes varying between 10 and 100 μm in diameter were observed right across the minimum diameter but with the largest holes near the centre of the specimen. The largest holes formed by rapid hole-growth and coalescence within inclusion colonies, and often had highly eccentric, elliptical cross-sections with the major axis of the ellipse normal to the specimen axis.

After strains of 0·10 to 0·15 the holes were larger and less eccentric (as shown in Fig. 11), although both the lateral and axial dimensions of the holes had increased significantly. The growth of these large individual holes finally culminated in failure initiation at a strain $\bar{e}^p = 0{\cdot}20$, as shown in Fig. 7.

A similar, although less comprehensive, study was performed on long transverse specimens of Q1, and hole nucleation was again observed to start after very small strains. Holes with eccentric, elliptical cross-sections were observed, but they differed from those observed in the short transverse direction in having their major axes in line with the specimen axis. Failure initiation finally occurred by hole coalescence as shown in Fig. 8.

4. DISCUSSION

4.1 *Hole nucleation*

The metallographic evidence suggests that, in these relatively high-strength steels, holes nucleate from large inclusions and inclusion colonies at very low strains. The simplest criterion for nucleation is that a critical radial stress is reached at the particle-matrix interface leading to decohesion. This stress would be reached at a lower strain in a steel having a high yield-stress than in one having a low yield-stress, and an increase in the tri-axiality of the stress-state might be expected to have a similar effect. A common mode of initiating holes, however, seems to be failure of the matrix surrounding the inclusion, and this is particularly the case when inclusions are close together, as in an inclusion colony. ORR and BROWN (1974) have studied the problem of a circular cylindrical inclusion in an elastic–plastic matrix in plane strain; and they have found that, in regions up to several diameters from the inclusion, both $\bar{e}^p$ and $\sigma_m/\bar{\sigma}$ are considerably higher than in the remote matrix, as shown in Fig. 12. In such regions, the microscopic carbides, which precipitation-harden the matrix, are subject to more severe stress-states and higher strains than the large inclusion, and voids may form on these precipitates and coalesce to form micro-cracks. However, as the

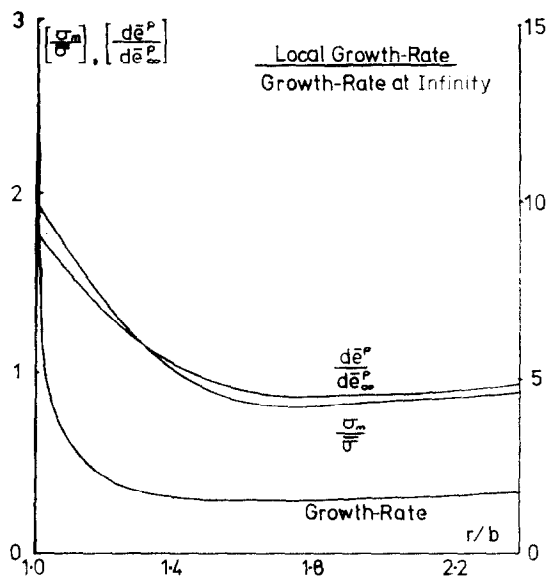

FIG. 12. Hole-growth amplification near a rigid inclusion.

formation of holes starts at very small strains, the dominant event leading to failure initiation in the high-strength steels is hole growth.

4.2 *Hole growth*

Considerable progress in the understanding of hole growth has been made through the theoretical models studied by BERG (1962), MCCLINTOCK (1968), and RICE and TRACEY (1969). MCCLINTOCK's (1968) model consists of a plastically-deforming matrix containing a regular array of pre-existing cylindrical holes of elliptical cross-section, each of which may be envisaged as sitting inside an identical cell as shown in Fig. 13.

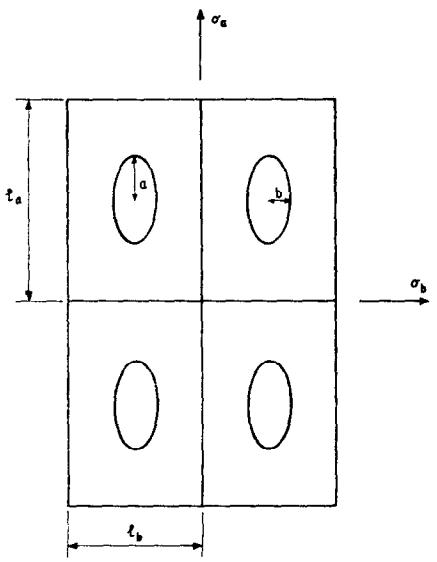

FIG. 13. MCCLINTOCK's (1968) fracture model.

The matrix deforms in generalized plane strain such that the strain parallel to the cylinder axis is uniform but non-zero. The dimensions of the cell, l_a and l_b, correspond to the hole spacings in these directions, and a and b are the corresponding semi-axes of the holes. Here, we have taken a to be the larger semi-axis and l_a to be the corresponding hole spacing. Following MCCLINTOCK's (1968) notation, introduce the two hole-growth factors F_a and F_b,

$$F_a = (a/l_a)/(a_0/l_a^0), \tag{6}$$

$$F_b = (b/l_b)/(a_0/l_b^0), \tag{7}$$

where the subscript '0' indicates an initial value. In MCCLINTOCK's (1968) model, failure occurs when there is a complete loss of cross-section, i.e. when $a = \frac{1}{2}l_a$ or $b = \frac{1}{2}l_b$ and

$$F_a = F_a^f = \tfrac{1}{2}(l_a^0/a_0) \tag{8}$$

or

$$F_b = F_b^f = \tfrac{1}{2}(l_b^0/b_0). \tag{9}$$

The equivalent plastic strain at failure by coalescence in the a-direction is given by

$$\bar{e}^{f} = \frac{(1-n)\ln(l_0/b_0)}{\sinh\left[\frac{1}{2}\sqrt{3}(1-n)\left(\frac{\sigma_a+\sigma_b}{\bar{\sigma}}\right)\right]+\frac{3}{4}\left(\frac{\sigma_b-\sigma_a}{\bar{\sigma}}\right)} \tag{10}$$

where σ_a and σ_b are the principal stresses in the remote matrix in the directions of the axes of the holes, and n is the strain-hardening exponent in the Ludwig power-law relation

$$\bar{\sigma} = \sigma_0(\bar{e}^{p})^{n}. \tag{11}$$

MCCLINTOCK (1968) neglected hole nucleation and identified the original hole-size with the inclusion size through the term $(l_0/2b_0)$. However, in both Q1 and HY130 this term is not *even approximately constant* in a given plane. For example, for HY130 in the rolling plane, $(l_0/2b_0)$ varies from 2 or less within an inclusion colony to a value of 10 or 20 between colonies, but the model does predict that holes within colonies will coalesce at very low strains. Instead of identifying the original hole size with the size of a single inclusion, we have identified it with the size of a large inclusion colony, 100 μm × 10 μm. The shape and size of one of these large holes at the failure initiation strain has then been calculated (using the Berg–McClintock method) for an A-notch specimen tested in the short and long transverse directions, and the results are given in Fig. 14. Dimensions have been introduced to facilitate direct comparison with the

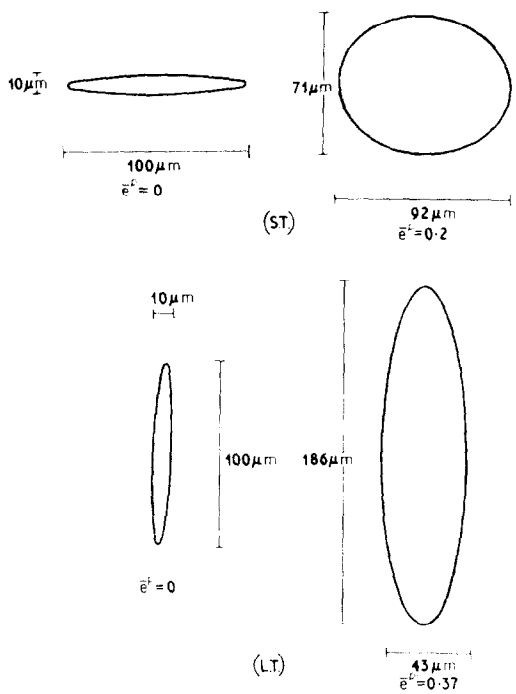

FIG. 14. Calculated hole shapes at failure initiation in Q1 taking the original hole size as that corresponding to an inclusion colony 100 μm × 10 μm.

corresponding micrographs in Figs. 7 and 8, and the agreement between the calculated and the observed hole shapes and sizes is good enough to confirm the appropriateness of taking the original hole size as that of an inclusion colony rather than a single inclusion.

With the assumption that the original inclusion and hole is elliptical in cross-section, it is possible to calculate the growth factors F_a and F_b for the central region of all the notches at the failure initiation strains. Results for an ellipse having an initial (major axis)/(minor axis) ratio of 10:1 are given in Table 3, and the essential steps in

TABLE 3. *Hole-growth factors at failure initiation*

Material	Notch	$\bar{e}^f$	$\sigma_m/\bar{\sigma}$	Transverse growth factor F_a	Axial growth factor F_b	F_aF_b	$(F_aF_b)^{\frac{1}{2}}$
	Uni-axial	1·05	0·33	11·7	1·40	16·38	4·05
Q1	*E*	0·63	1·26	6·23	1·37	8·54	2·92
L.T.	*A*	0·37	1·41	5·00	1·30	6·49	2·55
	C	0·23	1·69	5·49	1·33	7·30	2·70
	D	0·17	1·99	5·70	1·44	8·21	2·86
				factor F_b	factor F_a		
	Uni-axial	0·65	0·33	1·07	8·23	7·69	2·77
Q1	*A*	0·37	1·41	1·02	5·61	5·72	2·39
S.T.	*C*	0·12	1·69	1·02	5·20	5·3	2·30
	D	0·11	1·99	1·07	6·80	7·28	2·70

the calculation are given in the Appendix. The lateral growth factor in Table 3 refers to growth perpendicular to the specimen axis. In order to calculate growth factors in unnotched tensile specimens, account has been taken of changes in specimen geometry as necking proceeds, and the consequent change in stress-state at the centre of the neck. Geometry changes have, however, been ignored in the pre-notched specimens.

The lateral growth factors for failure initiation in the long transverse specimens are similar for all notches, and the average value is about 6. Thus, equations (8) and (9) would require the initial (hole spacing)/(radius) ratio (l_b^0/b_0) in a plane normal to the specimen axis to be about 12 for complete loss of cross-section to occur by hole coalescence in that plane. In the short transverse specimens, the lateral growth factors are again similar for all notches but the average value is only about 1·03. For hole coalescence in a plane normal to the specimen axis, the ratio (l_a^0/a_0) would have had to be about 2·1, requiring the holes in that plane to have been almost touching initially, and this is not in accord with the experimental observations. In addition, the simple coalescence model would seem to predict coalescence in the axial direction where the growth factors were comparable to those in the lateral direction in the long transverse specimens.

The photomicrographs of Figs. 7 and 8, which show the failure initiation event, indicate that uniform hole coalescence as originally envisaged does not occur, but that micro-cracking or some type of local flow instability occurs between the holes. The fact that the large holes do not grow homogeneously to touch one another at failure

initiation is in line with MCCLINTOCK's (1968) own observation that his model overestimates the ductility for a wide range of materials. If homogeneous hole growth is terminated by flow localization occurring at a critical hole spacing, then the discrepancy between the calculated and observed ductilities is reduced, and the stress-state dependence, as tested by the growth factors calculated for the range of notches, remains in accord with the experimental data. However, examination of photomicrographs (such as Fig. 7) also illustrates that, for real materials, hole coalescence does not occur in a single well-defined mode or on a single plane, in which case a growth factor averaged for all orientations seems more appropriate. In this context, it is interesting to note that the product of the growth factors, F_aF_b, which is also listed in Table 3 and represents the volume fraction of holes at failure initiation normalized with respect to the original volume fraction of holes, is quite similar for all the specimens, although the average value for tests in the short transverse direction is somewhat smaller than for tests in the long transverse direction. $(F_aF_b)^{\frac{1}{2}}$ is then also similar for all the notches and for both specimen orientations and represents an average growth-factor. If, then, failure initiates by flow localization at a constant volume fraction of holes, or after a critical dilation strain, or when a critical average growth factor $(F_aF_b)^{\frac{1}{2}}$ is reached, (all of which are equivalent), it seems natural to take $\sigma_m/\bar{\sigma}$ as the parameter to decide the stress-state rather than $(\sigma_a+\sigma_b)/\bar{\sigma}$ in (10).

Pursuing the idea that the conditions for failure initiation may be expressed in terms of global parameters, such as critical volume-fraction of holes and $\sigma_m/\bar{\sigma}$, the results of RICE and TRACEY (1969) may be used to obtain an approximate failure criterion. Their analysis of the growth of an initially spherical hole in a rigid/non-hardening matrix gave the rate-of-change of the mean hole radius R with plastic strain at high values of $\sigma_m/\bar{\sigma}$ as

$$dR/R = 0{\cdot}28\, d\bar{e}^p \exp(3\sigma_m/2\bar{\sigma}). \tag{12}$$

If it is assumed that the failure strain is inversely proportional to hole growth-rate, then the failure strain can be expressed as

$$\bar{e}^f = \alpha \exp(-3\sigma_m/2\bar{\sigma}), \tag{13}$$

where α is a material constant.

This expression is similar to MCCLINTOCK's (1968) criterion (10) with σ_m taken instead of $(\sigma_a+\sigma_b)$. For the materials tested here, and for the more severe stress-states, the second term in the denominator of (10) is small compared to the first, and the sinh function approximates well to half the exp function.

Equation (13) may be applied to the present tests by determining the constant α from $\bar{e}^f$ at one stress-state, and then using it to predict failure strains at other stress-states. If the result for the A-notch is used to determine α, then the predicted curves for the long and short transverse directions are as shown in Fig. 15 and they compare well with the data over much of the range of $\sigma_m/\bar{\sigma}$.

There are many materials in which appreciable plastic flow occurs before voids nucleate; and for such materials, equation (13) would have to be modified to

$$\bar{e}^f = \bar{e}_n + \alpha \exp(-3\sigma_m/2\bar{\sigma}), \tag{14}$$

where $\bar{e}_n$ is the void nucleation strain which may depend on stress-state. In an investigation on Swedish iron by HANCOCK (1976), $\bar{e}_n$ was found to be about 0·2 and

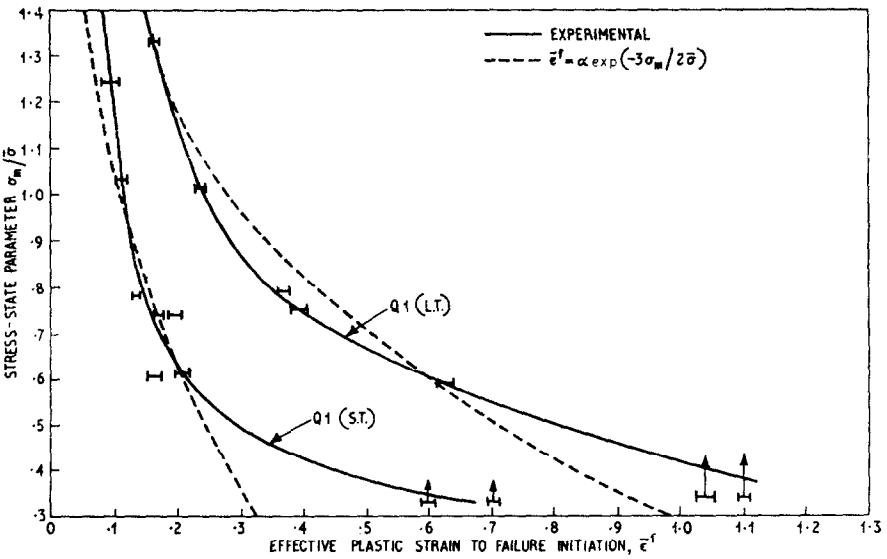

FIG. 15(a).

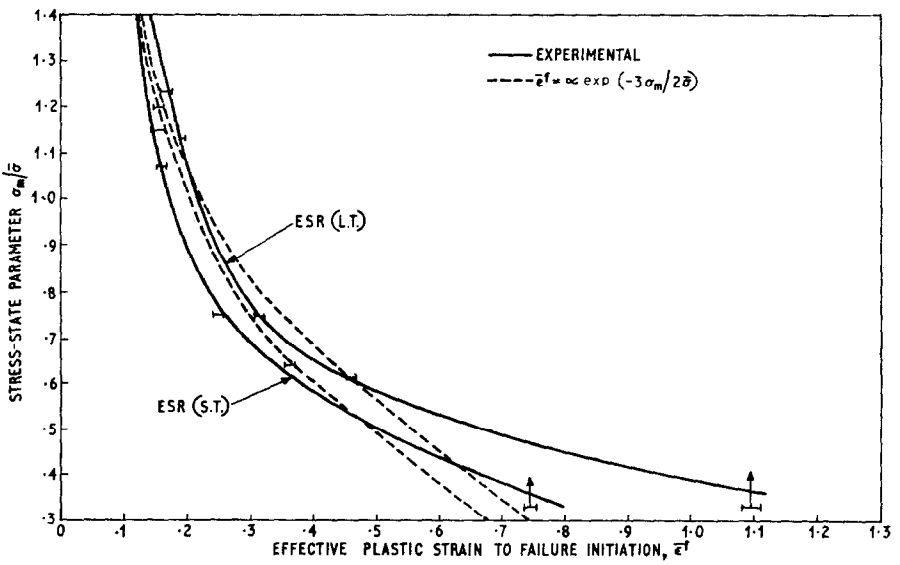

FIG. 15(b).

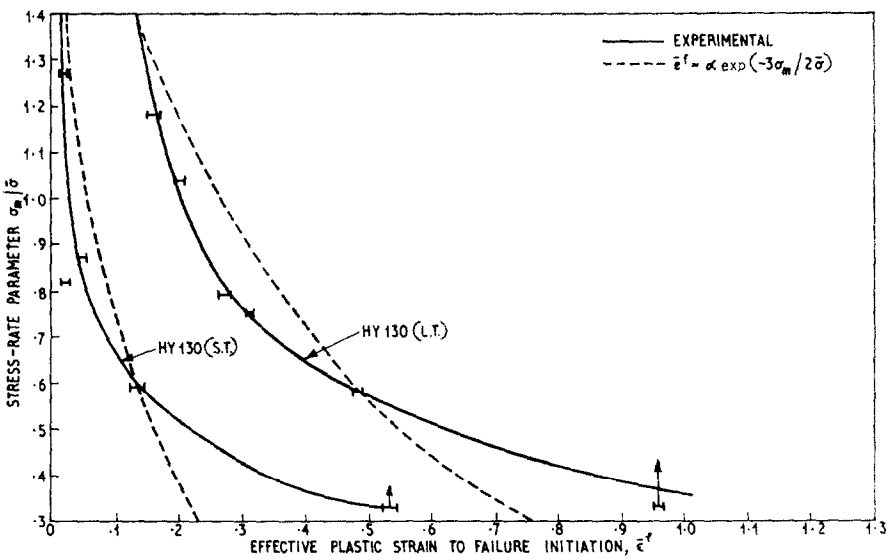

FIG. 15(c).

FIG. 15. (a) The effective plastic strain to initiate failure, $\bar{e}^f$, as a function of the stress state for Q1 tested in the long transverse and short transverse directions.
(b) The effective plastic strain required to initiate failure, $\bar{e}^f$, as a function of the stress state for ESR tested in the long and short transverse directions. (Note the lack of directionality in this steel compared with those prepared by more conventional techniques.)
(c) The effective plastic strain required to initiate failure $\bar{e}^f$, as a function of the stress state for HY130 tested in the long and short transverse directions. (Note that in the highly tri-axial states, HY130 S.T. fails at strains of the order of 0·02; whereas in uni-axial tension, failure occurs after a strain of the order of 0·65.)

independent of stress-state. Failure strains should thus be less dependent on stress-state than those for Q1 for which $\bar{e}_n$ is very small.

One of the features of BERG's (1962) analysis of hole growth, on which MCCLINTOCK's (1968) model and the growth factors in Table 3 are based, is that the semi-axes of the hole are expected to grow fastest in the direction of the maximum principal stress. In the high-strength steels, extensive hole growth occurs perpendicular to the major principal stress, particularly for material tested in the short transverse direction. Metallographic evidence, such as that shown in Fig. 16, suggests that holes grow not only by the simple continuum mechanics of individual hole growth, but also by coalescing with other smaller holes nucleating at carbides or small inclusions and growing rapidly under the influence of the stress fields of the large holes.

The effect may be illustrated by considering a single cylindrical hole of radius b in a rigid–plastic matrix subject to all-round tension and in generalized plane strain parallel to the axis of the cylinder. The strain parallel to the axis of the cylinder is adjusted to give $\sigma_m/\bar{\sigma} = 0{\cdot}75$ at large distances from the hole; this is the value of $\sigma_m/\bar{\sigma}$ in the centre of the A-notch specimen. Both the effective-strain concentration factor and the local tri-axiality are plotted as a function of distance from the hole in Fig. 17. On the same graph, the rate-of-growth of a small, initially spherical hole

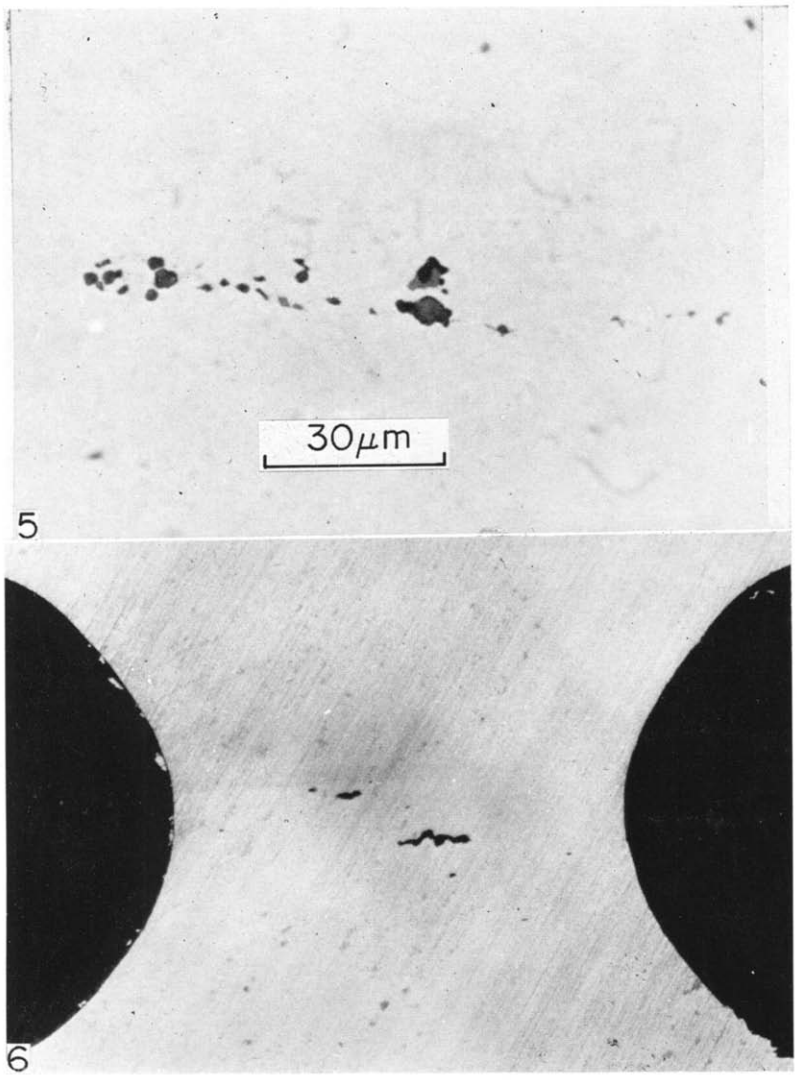

FIG. 5. An inclusion colony in Q1.

FIG. 6. A crack formed in the centre of a specimen after failure initiation.

[*facing p. 160*

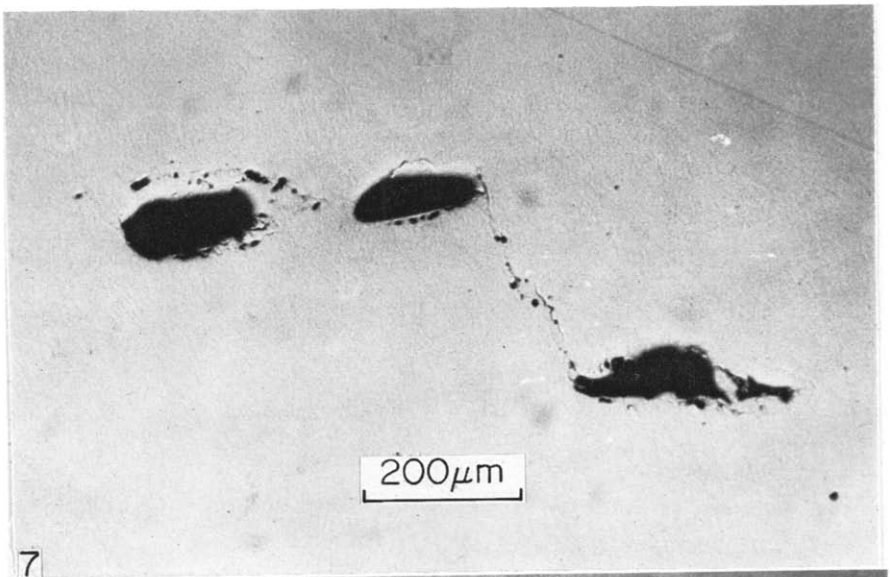

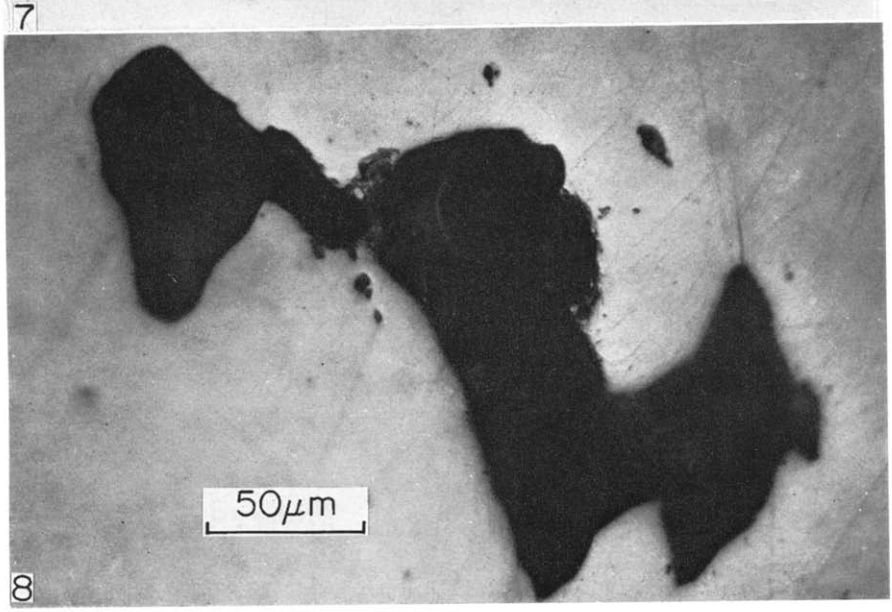

FIG. 7. Failure initiation in QI (A-notch) tested in the short transverse direction.

FIG. 8. Failure initiation in QI (A-notch) tested in the long transverse direction.

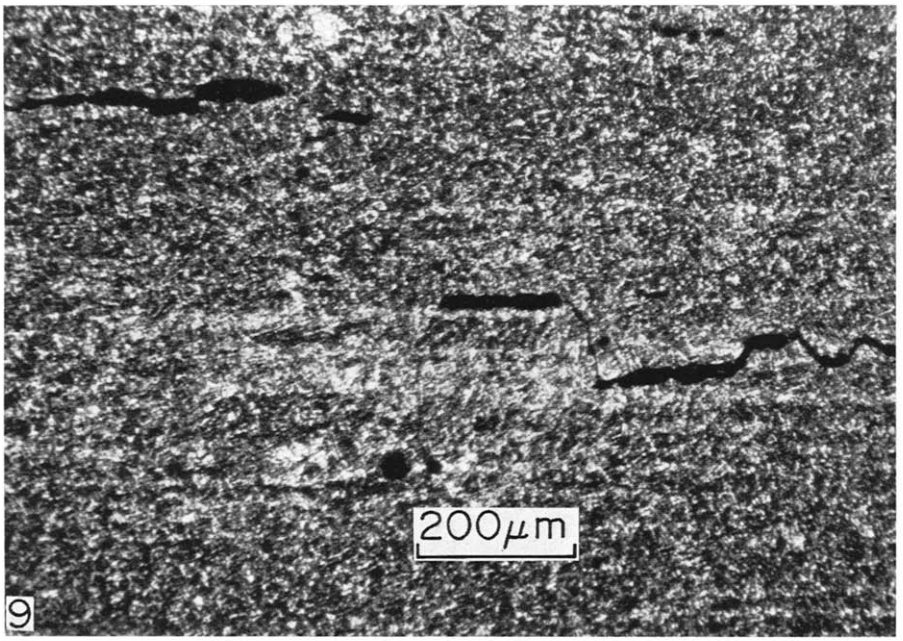

FIG. 9. The mechanism of failure in HY130 tested in the short transverse direction.

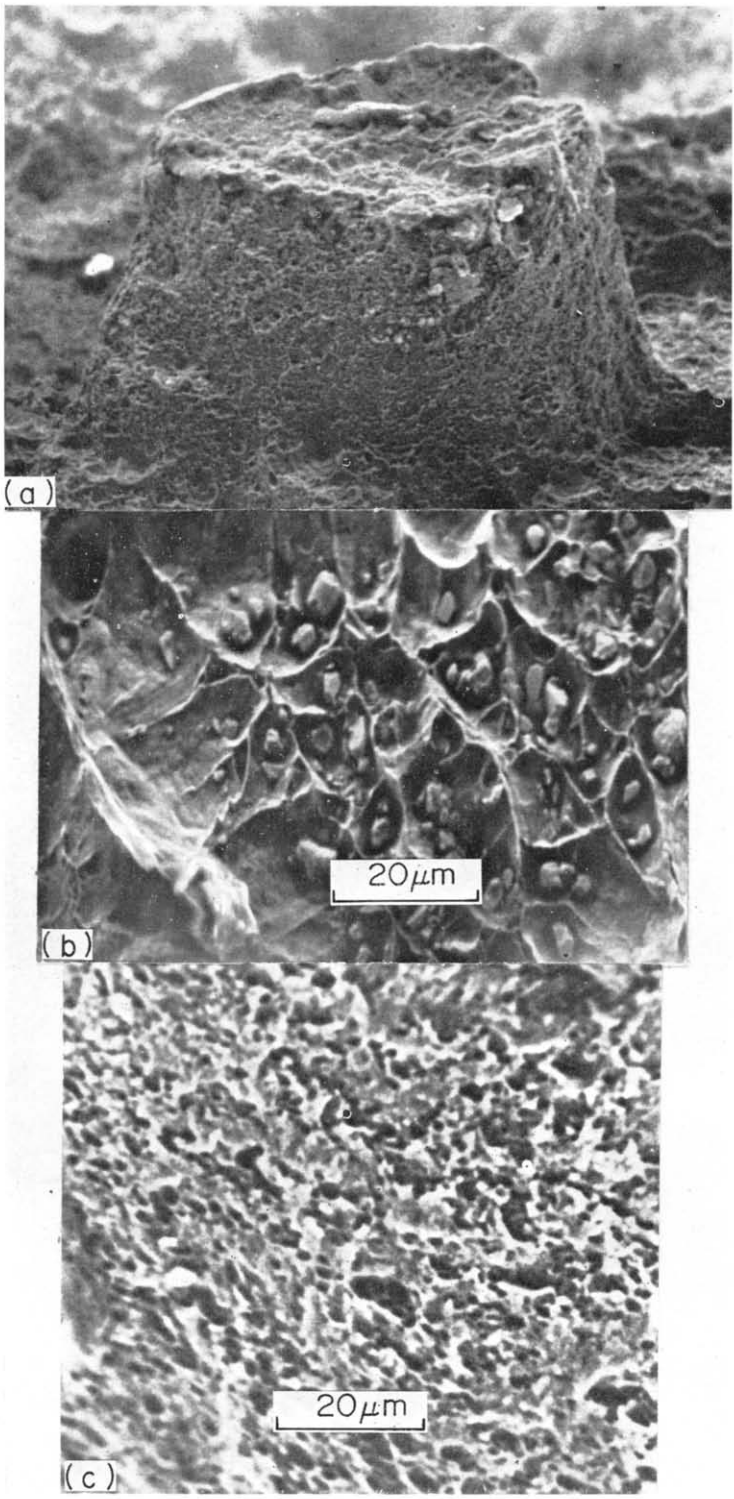

FIG. 10. (a) The fracture surface of HY130 tested in the short transverse direction showing the castellated fracture surface.
(b) Hole growth within an inclusion colony in HY130 (S.T.).
(c) Hole growth within the micro-cracked regions linking inclusion colonies in HY130 (S.T.).

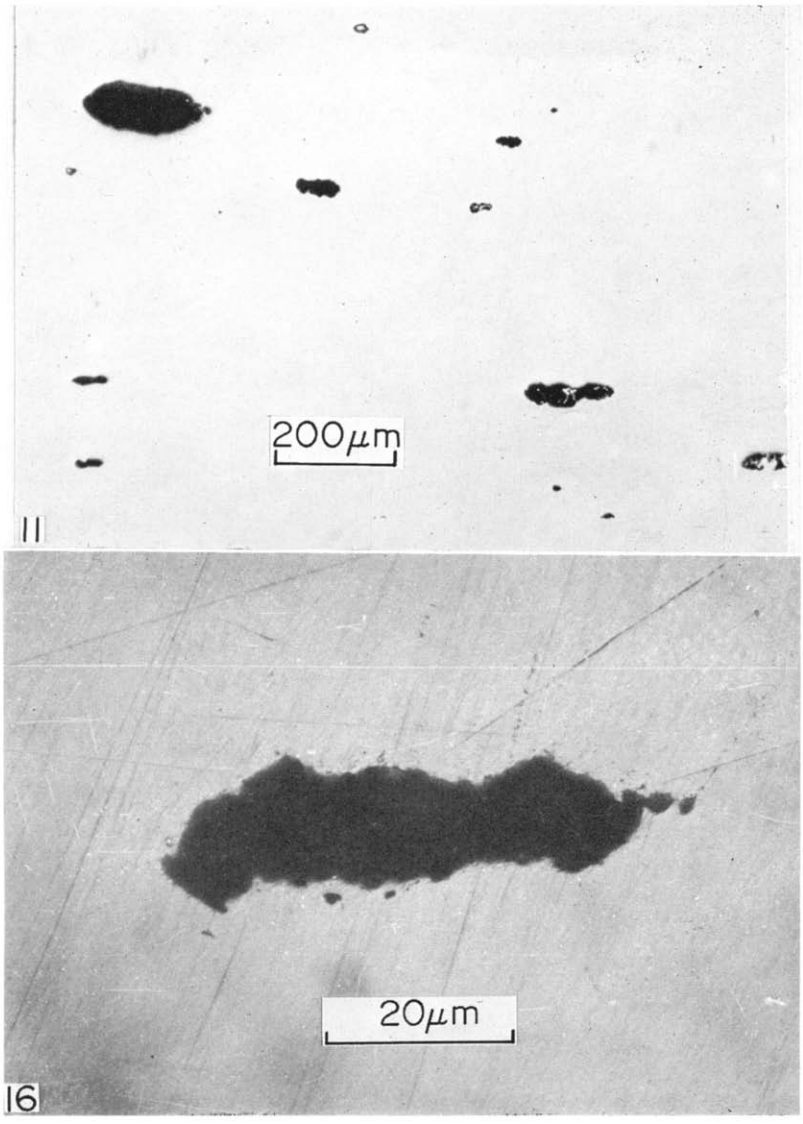

FIG. 11. Holes in Q1 (A-notch) short transverse direction at $\bar{e}^p = 0{\cdot}10$.

FIG. 16. Hole growth near a large void.

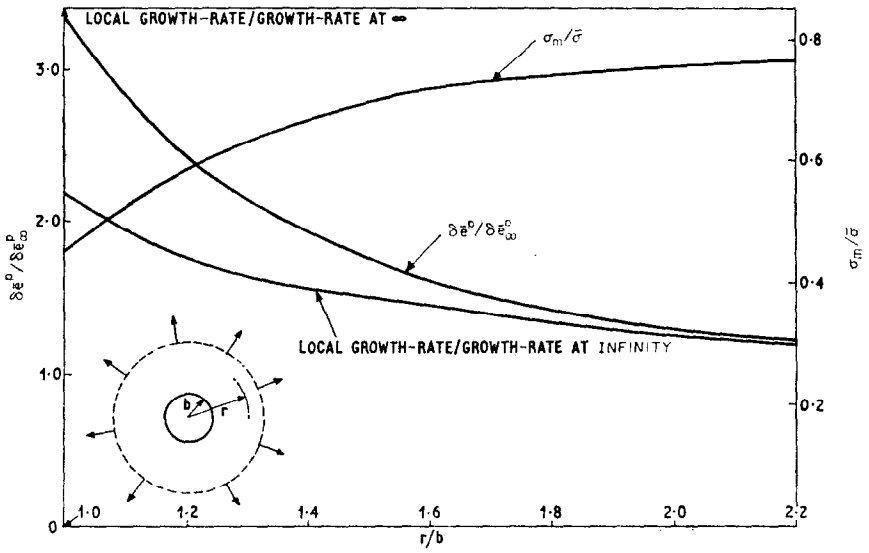

FIG. 17. Hole-growth amplification near a cylindrical hole.

divided by the rate-of-growth of a similar hole remote from the large hole is plotted as a function of distance from the large hole. The holes adjacent to a large hole grow almost twice as fast as those remote from it. The local amplification of hole growth allows large holes to grow by coalescing with smaller holes that nucleate and then grow in its stress field, and this effect is expected to be particularly pronounced for holes in the orientation shown in Fig. 16. It is with this *cautionary note* that the growth factors given in Table 3 are presented. In fact, the effect is expected to be most pronounced for the transverse growth factors F_a for Q1 tested in the short transverse direction, and it is expected to increase these values as well as the corresponding values of F_aF_b and $(F_aF_b)^{\frac{1}{2}}$ possibly bringing them more into line with the results for the long transverse direction.

4.3 *The linking-up of holes by flow localization*

Deformation before the marked drop in average stress, which has been defined as failure initiation, is characterized by homogeneous hole growth. After failure initiation, deformation is largely confined to the growth of a central crack in the minimum cross-section. The failure initiation event thus represents the transition between homogeneous hole growth and the first formation of a distinct crack. In contrast to MCCLINTOCK's (1968) model, the large holes do not actually touch one another at failure initiation but are often joined by micro-cracks as shown in Fig. 7. Such cracks result from smaller-scale hole growth processes (see Fig. 10(b)), probably based on carbides and small inclusions, and would seem to require a locally-severe stress-state and/or very high local strains. Such severe stress-states and high strains may arise by flow localization between the holes. For example, a possible mode of flow localization between cylindrical holes in plane-strain tension is that of two interlocking logarithmic

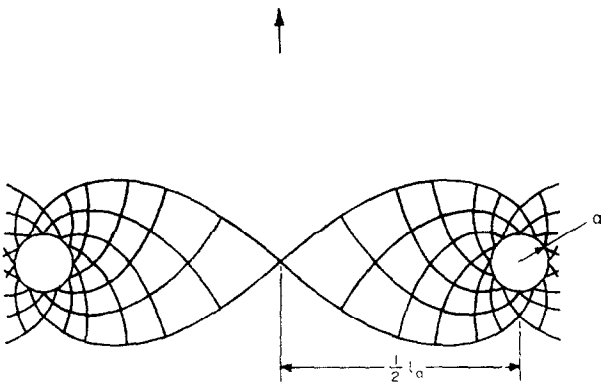

FIG. 18. A possible plane-strain slip-line field for localized flow, suggested by NAGPAL *et al.* (1973).

spiral slip-line fields (as shown in Fig. 18)). The stress-state midway between these holes is given by

$$\sigma_m/\bar{\sigma} = (1 + 2 \ln (l_a/2a))/\sqrt{3}, \tag{15}$$

where a is the hole radius and l_a the hole spacing, and it shows the elevation of stress-state which occurs in this region of high strain.

In studying the problem of flow localization, BERG (1970, 1972) has suggested, by analogy with the necking problem in sheets, that regions of flow localization should be bounded by rigid planes and lead to a load drop. In a notched tension specimen, the condition that the plane normal to the tensile axis does not deform is that the radial and hoop strains e_r, e_θ are zero. For a material deforming at constant volume, this implies that the axial strain is also zero; but for a material containing holes, axial strain may arise by dilation associated with hole growth. Thus, using the definitions of dilational strain,

$$de_{dil} = de_1 + de_2 + de_3, \tag{16}$$

and effective strain (equation (2)), it follows that

$$de_{dil} = \tfrac{3}{2} d\bar{e}. \tag{17}$$

In order to evaluate (17) rigorously, a dilational stress–strain relationship is required and this is not available. However, in order to get a feel for the implications of the result, it is worthwhile making some approximations. For a rigid–plastic material containing approximately spherical holes, the Rice–Tracey result of (12) for the growth of a spherical hole may be used to calculate very approximately the dilation of a volume fraction f of holes. Substitution into (17) gives the volume fraction of holes that is required for localization as a function of stress-state, i.e.

$$f = [0{\cdot}56 \exp (3\sigma_m/2\bar{\sigma})]^{-1}. \tag{18}$$

If there is a highly tri-axial stress-state, for example $\sigma_m/\bar{\sigma} = 1{\cdot}4$, then (18) suggests that only a 22% volume fraction of holes is required for localization, whereas for

$\sigma_m/\bar{\sigma} = 0{\cdot}5$, an 85% volume fraction is necessary. This suggests that in very dirty or highly precipitation-hardened materials at severe stress-states, flow localization may occur as soon as the holes are formed. Furthermore, if the material originally contained a volume fraction of holes, f_0, and if the simplifying approximation that the holes remain spherical (as is the case for highly tri-axial stress-states) is again made, then the amount of uniform strain to produce flow localization is

$$\bar{e}^p = 1{\cdot}2(0{\cdot}58 - \ln f_0 - 3\sigma_m/2\bar{\sigma}) \exp(-3\sigma_m/2\bar{\sigma}), \tag{19}$$

and this indicates a very stress-state sensitive fracture process. However, although the expressions developed for the growth of isolated holes in an infinite matrix are probably good approximations to the growth of widely-separated holes, it seems likely that they will over-estimate the rate at which holes grow in a porous material. A problem also arises, in that without plastic stress–strain relations showing dilation, it is not possible to determine the stress-state in the porous material before localized flow occurs.

The strain-state in the notch tension-specimens is assumed to be that of uni-axial tension, and the stress-state is unlikely to be less severe than that of uniaxial tension ($\sigma_m/\bar{\sigma} = \frac{1}{3}$); it may, however, be less severe than that calculated with the Bridgman results for an incompressible material. The present results seem to favour localization at a critical local volume fraction of holes and do not indicate such a decreased volume fraction of holes in the severe notches at failure initiation as suggested by (18) and (19).

Rigid planes bounding a region of localized flow do not occur right across the specimen but the initiation event occurs within a small volume at the centre of the specimen. To this extent, the mode of flow localization at failure initiation leading to (17) and (18) is over-simplified. However, a similar mode of flow localization may occur within inclusion colonies and produce very high strains which lead to rapid hole-growth and coalescence for very small applied strains. In this case, the material outside the colony does not become rigid, but the difference between the large effective plastic strain increments inside the colony and the small strain increments outside the colony is accommodated by the dilation of the material inside the colony as the holes grow.

It may also be noted that hole growth during flow localization has been studied by NAGPAL, MCCLINTOCK, BERG and SUBUDHI (1967) using interacting slip-line fields for arrays of holes. These show a higher transverse growth rate than expected for isolated holes growing homogeneously, and this corresponds well to the growth of holes within inclusion colonies in HY130 (shown in Fig. 10(b)) in which the transverse growth-rate is comparable with the axial growth-rate.

The same material HY130 tested in the short transverse direction also shows a very distinctive mode of failure initiation, in which flow localization occurs in shear bands between cracked inclusion colonies, as idealized in Fig. 19. Here, the two halves of the specimen move apart as rigid blocks leaving the castellated fracture surface shown in Fig. 10. For a non-hardening material in uniaxial tension, an upper bound on the load for homogeneous flow is obtained by assuming uniform distribution of strain, i.e.

$$P_h \leqslant \sigma_y w \tag{20}$$

where σ_y is the yield stress in tension, and P_h is the load for a unit cell of width w and for unit thickness. When flow is localized in shear bands, as in Fig. 19, the associated

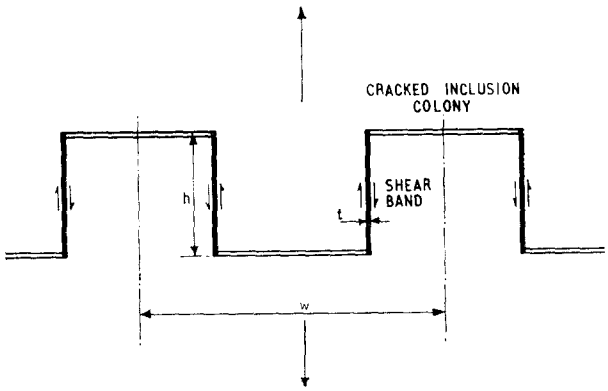

FIG. 19. The idealized fracture mode of HY130 tested in the short transverse direction.

load P_l may be estimated by using the upper-bound limit design theorem to obtain

$$P_l \leq \frac{2}{\sqrt{3}} \sigma_y h \tag{21}$$

The quantities w and h in (20) and (21) are defined in Fig. 17.

As MCCLINTOCK (1967) has pointed out in a related shear-band analysis, the first condition for flow localization to occur is that $P_l \leqslant P_h$, and, strictly speaking, the upper bound on P_l should be compared with a lower bound on P_h. However, a comparison of upper bounds gives a useful approximation and suggests that for flow to localize,

$$h \leq \tfrac{1}{2}\sqrt{3}w. \tag{22}$$

This condition is clearly satisfied in the photomicrographs of Fig. 10. For localized flow to occur, the mode must also lead to a stationary load or to a load drop. The area A of ligament resisting shear between cracked inclusion colonies reduces as the inclusion surfaces separate, but this reduction in area may be offset by work-hardening of the material. If τ is the value of the shear stress in the bands when flow localizes, then

$$P_l = 2A\tau. \tag{23}$$

For localization,

$$dP_l = 2\tau dA + 2Ad\tau \leq 0. \tag{24}$$

Since

$$dA = -2td\gamma, \tag{25}$$

where t is the thickness of the band and $d\gamma$ is the shear strain in the band, the work-hardening condition for this mode of flow localization is

$$d\tau/d\gamma = d\bar{\sigma}/d\bar{e}^p \leq 2t\tau/h, \tag{26}$$

i.e.

$$d\bar{\sigma}/d\bar{e}^p \leq 2\bar{\sigma}t/\sqrt{3}h. \tag{27}$$

For HY130, $d\bar{\sigma}/d\bar{e}^p \approx 1$ kN/mm^2 and $\bar{\sigma} \approx 1$ kN/mm^2; and thus, as $t \ll h$, the condition cannot be fulfilled with the current strain-hardening rates and seems only to be met by materials with exceptionally low strain-hardening rates, unless the strain-hardening rate of the band is reduced by porosity. As failure in the bands occurs by small-scale hole growth, this seems quite likely, and again emphasizes the importance of 'second generation' small-scale hole growth between large holes in these high-strength steels. Thus, although the holes which develop from large inclusions may not always grow until they coalesce completely, the strain concentration associated with their growth (as illustrated in Fig. 17) favours the nucleation and rapid growth of voids from precipitate particles within the stress field of the large holes. The amount of small-scale hole growth and extent of local damage may be sufficient to join the larger holes directly. However, as such precipitates often control the strain-hardening characteristics of the material and the development of holes on the precipitates reduces the strain-hardening rate (ASHBY, 1966), small-scale hole growth also favours flow localization in shear bands, as noted in Fig. 9.

4.4 *Application of the data and the material-size parameter*

The data presented here are important in that they allow the initiation of failure to be predicted in multi-axial stress-fields. However, in order to predict failure initiation in non-uniform stress fields, such as those ahead of cracks and flaws, it is not a sufficient condition for failure initiation that a strain which is a function of stress-state is exceeded at a point. *Failure initiation must involve a minimum amount of material which is characteristic of the scale of physical events involved.* For example, in Q1, failure initiates by the linking of two or more of the large holes formed from inclusion colonies, and such a failure mode would not be possible over distances smaller than the inclusion spacing. This scale of physical events has been characterized by a material-size parameter, which has been taken as 200 μm for Q1, and has enabled MACKENZIE, *et al.* (1976) to predict the critical stress intensity factor and critical defect sizes for the initiation or failure ahead of cracks in small-scale yielding.

5. CONCLUSIONS

The ductility of high-strength steels depends markedly on the stress-state which may be characterized by $\sigma_m/\bar{\sigma}$, basically in accord with MCCLINTOCK's (1968) model of ductile failure. Although this model, which is based on the growth of discrete holes in a homogeneous continuum, over-simplifies the actual mechanisms of failure in high-strength steels, it contains many of the essential features of the process. Specifically, complications to simple models arise when an important mechanism of hole growth from large inclusions is that of coalescing with micro-voids generated from precipitates within the stress field of the large holes. On this basis, the hole-growth equations often under-estimate the rate at which large holes grow; particularly for elliptical holes oriented with their major axes normal to the largest principal stress. However, more important is the fact that the large holes often do not coalesce completely but are linked by micro-cracks which are a result of a second generation of small-scale hole growth based on carbides or other precipitates between the large holes. In order to produce the necessary amount of small-scale hole growth, high local

strain and/or an enhanced stress-state is required; and these conditions may be produced by a plastic instability, resulting in flow localization between the large holes. The size, shape and spacing of the large holes when this process starts is clearly important. Calculation of these parameters for Q1 and comparison with experimental observations suggests that failure initiation in this material may occur at a critical volume fraction of large holes. This is equivalent to a critical hole spacing averaged over all orientations, and may correspond to the observation that hole coalescence does not occur on a single well-defined plane. The mechanism of flow localization and failure initiation is not unique, and it varies with material and the orientation of the stress system with respect to the material axes. Notably, in this work, HY130 tested in the short transverse direction failed by flow localization in shear bands between the large holes, a process in which small-scale hole growth again appears to be important.

The present work has again emphasized the highly directional properties of wrought steels which MCCLINTOCK (1968) has referred to in his well-known model of ductile failure. Directionality may be attributed to the variation in hole or inclusion spacing from plane to plane. However, the work presented here suggests that an equally important factor is the distribution of inclusions within a given plane, which for real materials is highly irregular. This leads to extensive hole coalescence within inclusion colonies by a process akin to flow localization very early along the stress–strain curve, and produces highly eccentric holes. The dilation rate is a function of stress-state: but for eccentric holes, it also depends markedly on the orientation of the holes with respect to the stress system.

As emphasized in earlier discussion, high dilation-rates result when the major principal stress is aligned with the minor semi-axis of the elliptical hole; very much lower dilation-rates result when the major principal stress is aligned with the major axis of the hole. Thus, if failure initiation occurs when a critical volume fraction of holes is reached, or the growth factor averaged over all orientations reaches a critical value, it will occur at a lower strain for specimens tested in the short transverse direction than for specimens tested in the long transverse direction, due to the very much higher dilation-rate in the former case.

ACKNOWLEDGMENT

This work has been carried out with the financial support of the Procurement Executive, Ministry of Defence, London, United Kingdom.

REFERENCES

ASHBY, M. F. 1966 *Phil. Mag.* **14,** 1157.

BERG, C. A. 1962 *Proceedings of the Fourth U.S. National Congress of Applied Mechanics* (University of California, Berkeley, June 18–21, 1962), (edited by ROSENBERG, R. M.), Vol. Two, p. 885. American Society of Mechanical Engineers, New York.

1970 *Inelastic Behavior of Solids* (edited by KANNINEN, M. F., ADLER, W. F., ROSENFIELD, A. R. and JAFFEE, R. I.), p. 171. McGraw–Hill, New York.

1972 *J. Res. Nat. Bur. Stand.* **76C,** 33.

BRIDGMAN, P. W.	1952	*Studies in Large Plastic Flow and Fracture*, p. 9. McGraw-Hill, New York.
EARL, J. and BROWN, D. K.	1976	*Eng. Fract. Mech.* In press.
HANCOCK, J. W.	1976	*Proceedings of the Second International Conference on the Mechanical Behavior of Materials* (Boston, August 16–20, 1976), (edited by N. E. PROMISEL *et al.*). In press.
MCCLINTOCK, F. A.	1956	*Proceedings of the International Conference on Fatigue of Metals* (London, 10–14 September, 1956. New York, 28–30 September, 1956), p. 538. Institution of Mechanical Engineers, London.
	1967	*Ductility.* (Papers presented at a Seminar of the American Society for Metals, October 14 and 15, 1967), Ch. 9. American Society for Metals, Metals Park, Ohio.
	1968	*J. appl. Mech.* **35**, 363.
MACKENZIE, A. C., HANCOCK, J. W. and BROWN, D. K.	1976	*Eng. Fract. Mech.* To be published.
NAGPAL, V., MCCLINTOCK, F. A., BERG, C. A. and SUBUDHI, M.	1973	*Foundations of Plasticity* (International Symposium, Warsaw, August 30–September 2, 1972), (edited by SAWCZUK, A.), p. 365. Noordhoff, Leyden.
RICE, J. R. and TRACEY, D. M.	1969	*J. Mech. Phys. Solids* **17**, 201.
RITCHIE, R. O., KNOTT, J. F. and RICE, J. R.	1973	*Ibid.* **21**, 395.
ORR, J. and BROWN, D. K.	1974	*Eng. Fract. Mech.* **6**, 261.

APPENDIX

Calculation of Hole Size and Shape following the Berg–McClintock Method

Consider an elliptical hole in a plate of linear viscous material and under principal stresses σ_1 and σ_2 inclined at angle α' to (x, y)-axes in the plane of the plate. The ellipse has major and minor semi-axes, a and b as shown in Fig. A.1, and has mean radius

$$R = \tfrac{1}{2}(a+b). \tag{A.1}$$

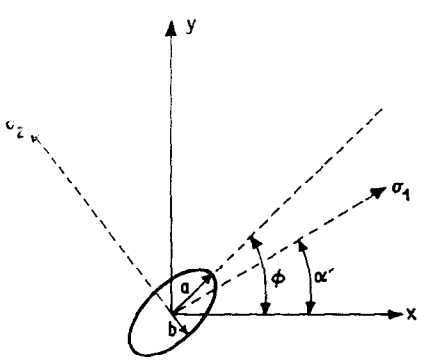

FIG. A.1. Elliptical hole in an infinite plate.

The eccentricity and orientation of the ellipse is defined through a *complex number m*, where the eccentricity as defined by Berg is

$$|m| = (a-b)/(a+b), \tag{A.2}$$

and the inclination Φ of the major axis of the ellipse to the x-axis is

$$\Phi = \tfrac{1}{2} \arg m. \tag{A.3}$$

BERG (1963) solved the finite strain problem of the growth of such a hole; and, excluding the case in which $(\sigma_1+\sigma_2) = 0$, his results may be summarized by

$$m_{t'} = (m_0 - \{(\sigma_1-\sigma_2)/(\sigma_1+\sigma_2)\} \exp(2i\alpha')) \exp(-2(1+\kappa)(\sigma_1+\sigma_2)t'/8\mu) + \\ + \{(\sigma_1-\sigma_2)/(\sigma_1+\sigma_2)\} \exp(2i\alpha'), \tag{A.4}$$

$$R_{t'} = R_0 \exp((1+\kappa)(\sigma_1+\sigma_2)t'/8\mu), \tag{A.5}$$

where t' represents time, the subscript '0' represents an initial value, the subscript 'O'' indicates the appropriate value of the subscripted variable at time t', μ is viscosity, and κ is a constant.

The growth of an elliptical hole, whose semi-major axis and the stress σ_1 lie in the x-direction, is then given by

$$\Phi = \alpha' = 0. \tag{A.6}$$

The growth of a hole, when its semi-minor axis and the stress σ_1 lie in the x-direction, is given by

$$\Phi = \tfrac{1}{2}\pi, \qquad \alpha' = 0. \tag{A.7}$$

Equations (A.3) and (A.4) have been adapted for generalized plastic plane strain by MCCLINTOCK (1968). In generalized plane strain, a uniform strain $e_3^p(\neq 0)$ is applied perpendicular to the (xy)-plane.
This gives

$$R = R_0 \exp[(\tfrac{1}{2}\sqrt{3}\bar{e}^p/(1-n) \sinh(\tfrac{1}{2}\sqrt{3}(\sigma_1+\sigma_2)(1-n)/\bar{\sigma}) - \tfrac{1}{2}e_3^p] \tag{A.8}$$

$$m = \{(\sigma_1-\sigma_2)/(\sigma_1+\sigma_2)\} \exp(2i\alpha') + (m_0 - \{(\sigma_1-\sigma_2)/(\sigma_1+\sigma_2)\} \times \\ \times \exp(2i\alpha')) \exp\{-\sqrt{3}\bar{e}^p/(1-n)\} \times \sinh(\tfrac{1}{2}\sqrt{3}\bar{e}^p(1-n)(\sigma_1+\sigma_2)/\bar{\sigma}) \tag{A.9}$$

In order to apply these results to the calculations of hole growth in a notched tensile-specimen, the stresses σ_1, σ_2 are taken as the axial and hoop stresses σ_z, σ_θ respectively. At the centre of the specimen these stresses can be calculated from

$$\sigma_z = \bar{\sigma}(1+\ln(\tfrac{1}{2}a/R+1)), \tag{A.10}$$

$$\sigma_\theta = \bar{\sigma}(\ln(\tfrac{1}{2}a/R+1)). \tag{A.11}$$

Noting that the radial strain is independent of the radial co-ordinate r, the radial strain may by identified with e_3 in (A.7) and calculated from the integrated form of the Lévy–Mises flow-rule

$$e_r^p = (\bar{e}^p/\bar{\sigma})\{\sigma_r - \tfrac{1}{2}(\sigma_z+\sigma_\theta)\}. \tag{A.12}$$

The strain $\bar{e}^p$ may be obtained from the change in specimen dimensions given in (5), and the stresses normalized with respect to the equivalent flow-stress from use of

(A.10) and (A.11). The stresses and strains are then substituted into (A.8) and (A.9) with $n = 0{\cdot}2$ and $\alpha' = 0$ or $\alpha' = \frac{1}{2}\pi$ to calculate the eccentricity and mean radius of the hole. The semi-axes can then be calculated by solving (A.1) and (A.2) simultaneously.